Journal of Electroanalytical Chemistry 857 (2020) 113754

Contents lists available at ScienceDirect

Journal of Electroanalytical Chemistry

journal homepage: www.elsevier.com/locate/jelechem

Effect of temperature on the ethanol electrooxidation at $PtNi_{rich}@Pt_{rich}Ni$/C catalyst in acidic and alkaline media

Lays S.R. Silva [a,b], Iasmim G. Melo [a], Cristiano T. Meneses [c], Franz E. Lopez-Suarez [d,*], Katlin I.B. Eguiluz [a,b], Giancarlo R. Salazar-Banda [a,b]

[a] Electrochemistry and Nanotechnology Laboratory - LEN, Instituto de Tecnologia e Pesquisa - ITP, Av. Murilo Dantas, 300, Aracaju, SE, Brazil
[b] Postgraduate Programme in Process Engineering - PEP, Universidade Tiradentes, Av. Murilo Dantas, 300, Aracaju, SE, Brazil
[c] Department of Physics, Universidade Federal de Sergipe, Campus Itabaiana, Av. Ver. Olimpio Grande S/N, Itabaiana, SE, Brazil
[d] GIPSI Group/Department of Chemical Engineering, Universidad de Bogotá Jorge Tadeo Lozano, Street 4 # 22-61, 110311 Bogota, Colombia

ARTICLE INFO

Article history:
Received 11 September 2019
Received in revised form 19 November 2019
Accepted 9 December 2019
Available online 10 December 2019

Keywords:
Electrocatalysis
Reaction kinetics
Core-shell
Fuel cells

ABSTRACT

The understanding of the kinetics of the electrochemical oxidation of ethanol at high temperatures is essential for the optimization of direct ethanol fuel cells. Here, we study the kinetics of the ethanol oxidation reaction between 25 and 65 °C using $PtNi_{rich}@Pt_{rich}Ni$ catalysts supported on functionalized carbon, in acid and alkaline solutions. The characterization of the catalysts made by X-ray diffraction, scanning–transmission electron microscopy, energy dispersive X-ray spectrometry, selected area electron diffraction, and cyclic voltammetry suggest the formation of core–shell nanostructures of Ni and Pt, while some nanoparticles can be forming alloys. The CO-stripping study reveals that the CO_{ads} oxidation shifts to negative potentials when the temperature increases, in both 0.5 M H_2SO_4 and 0.5 M KOH media. However, in alkaline electrolyte, the lower current density at higher temperatures is associated with the CO_{ads} oxidation. Similar behavior is observed for ethanol oxidation reaction until a temperature of 65 °C. The activation energy values calculated by linear sweep voltammetry are 16.28–14.54 kJ mol^{-1} in acidic media and 9.25–7.97 kJ mol^{-1} in alkaline media. Therefore, the understanding of the kinetics of the ethanol oxidation in the conditions and catalysts studied here could help in selecting the catalytic components and operating environment, which result in enhanced efficiencies toward both CO_{ad} and ethanol oxidation.

1. Introduction

The development of a sustainable society needs wide-spread applications of renewable, reliable, and cost-effective energy technologies [1]. The primary way to achieve this goal is beginning by diminishing our dependence on combustible fossil fuels [2,3] Direct ethanol fuel cell (DEFC) is an exciting technology since ethanol has several advantages such as non-toxicity, high energy efficiency, simple production from biomass fermentation, and ease storage and transport [4–7].

The commercial implementation of DEFCs has been challenging due to the Pt electrocatalyst used in the cell is a precious and scarce metal, also having low catalytic activity and weak stability [8]. The ethanol oxidation reaction (EOR) can follow parallel pathways leading to strongly adsorbed intermediates, such as acetaldehyde and acetate, which poisoning the electrocatalyst surface, thus reducing the efficiency of the FC [7,9]. On bulk Pt and Pt/C, the break of the C—C bond during the EOR is hard, producing acetaldehyde ($2e^-$) or acetic acid ($4e^-$) by incomplete ethanol oxidation [10,11].

The development of highly active, stable, and efficient Pt electrocatalysts for anodic oxidation is a pressing research matter [8,12–14]. The introduction of low-cost *3d* transition metals such as Co, Fe, and Ni as well as the design of innovative morphologies are performed to diminish the cost and improve the activity of the catalyst since exiting a synergy between different components (geometric and electronic effect) [15–20].

The electrocatalytic reactions occur on the surface of catalysts [21] and therefore, this parameter depends on their surface properties [16,22]. High catalytic activities can be obtained by tuning the composition [15] and the surface structure [23,24]. Various studies have focused on the effect of the temperature on surface coverage of CO and other intermediates, on anion adsorption and oxide coverage, on turnover rate enhancements, and the onset potential shifts [15,25–31].

Barbosa et al. [30] observed that a decrease in temperature decreases the current density (from 16.3 mA cm^{-2} at T = 25 °C to 0.8 mA cm^{-2} at T = −15 °C) in 0.1 M NaOH +0.5 M and shifts the onset potential of the EOR to positive values. Bach Delpeuch et al. [34] determined the activation energy (E_a) for ethanol oxidation on Pt/C, Pt–Rh/C and Pt/Rh–SnO_2/

* Corresponding author.
E-mail addresses: franzedwin@gmail.com (F.E. Lopez-Suarez), katlin.eguiluz@pq.cnpq.br (K.I.B. Eguiluz).

https://doi.org/10.1016/j.jelechem.2019.113754
1572-6657/

C electrodes in 0.5 M H_2SO_4 + 0.1 M ethanol. The E_a values were potential-dependent, and the CO-stripping onset potential was lower at Pt–Rh/C and Pt/Rh–SnO_2/C than at Pt/C. Moreover, the CO peak shifts negatively when the temperature increases. The modification on the structure of catalyst could improve the electro-oxidation of nanostructures with two-dimensional (2D) such as nanosheets, which have demonstrated enhancement in the electro-oxidation of several molecules. For instance, Lv et al. [32] found that trimetallic PdPtCu nanosheets synthesized under ambient enhanced electrocatalytic performances compared to materials with 0-D nanostructures.

Here, we investigated the ethanol electrooxidation reaction on developed $PtNi_{rich}$@Pt_{rich}Ni/C (named as only Ni@Pt/C hereafter) nanoparticles using an approach for determining the E_a values in acidic (H_2SO_4) and alkaline (KOH) media by linear sweep voltammetry (LSV) analysis in a temperature range of 25 °C ≤ T ≤ 65 °C. The LSV data are used to create Arrhenius plots and the chronoamperometry analysis is used for determining the effect of the temperature in the extent of catalyst poisoning. The impact of the synthesis temperature of the Ni@Pt/C nanoparticles on their electrochemical activity was also evaluated.

2. Experimental

2.1. Functionalization of carbon black Vulcan XC-72R

The procedure for surface treatment of carbon black Vulcan® XC-72R (Cabot Corporation, BET: 237 m^2/g) is similar to the reported by Xing for multi-walled carbon nanotubes [33]. In a typical experiment, carbon black (200 mg) is mixed with 188 mL of HNO_3 (≥65%, Sigma–Aldrich), 160 mL of H_2SO_4 (≥98%, Sigma–Aldrich) and 12 mL of ultrapure water in a 500 mL Pyrex glass flask. The dispersion was sonicated for 3 h. Finally, the mixture obtained was filtered and washed several times with ultrapure water (Gehaka model MS 2000 system, 18.2 MΩ·cm) and then dried at 60 °C for 8 h. In Fig. S1 is shown the scheme of the carbon functionalization and core-shell nanoparticles synthesis.

2.2. Synthesis of core-shell nanoparticles

Ni@Pt (25% of Ni and 75% of Pt, both atomic) nanoparticles were deposited on functionalized carbon by a chemical reduction of Nickel chloride (Cl_2Ni, ≤100%, Sigma–Aldrich) and chloroplatinic acid ($H_2PtCl_6.6H_2O$, ≥37.50%, Sigma–Aldrich) in ethylene glycol–water solution using a sequential synthetic method. Briefly, 0.75 mL aqueous solution of 0.0841 M (Cl_2Ni), 4.25 mL of ultrapure water, and 160 mg of carbon were mixed with 20 mL EG. The mixture was then ultrasonically homogenized for 4 h. Later, the reduction is performed at 80 °C for 24 h under constant stirring, and the mixture is cooled to room temperature, filtered, washed with ultrapure water and dried at 80 °C for 15 h (Ni/C). This procedure was repeated to coat the Ni/C nanoparticles formed in the previous step with Pt to obtain Ni@Pt/C.

2.3. Catalysts characterizations

X-ray powder diffraction (XRD) analyses were carried out using a PANalytical Empyrean diffractometer with Cu Kα radiation (λ = 0.15418 nm) at 40 kV and 40 mA. The diffraction data were recorded for 2θ angles between 30° and 85°. The Ni@Pt/C catalysts were also characterized by scanning–transmission electron microscopy (STEM), FEI Tecnai G2F20, equipped with a bright field (BF), an annular dark field (ADF) STEM detector, energy dispersive X-ray spectrometry (EDX), and selected area electron diffraction (SAED) operated at 200 kV. Particle size distribution for Ni@Pt/C catalysts was constructed using about 310 particles, and the measurement was carried out using ImageJ software.

2.4. Electrochemical measurements

The electrochemical measurements were carried out in a standard three-electrode cell using Autolab Model PGSTAT 302N potentiostat/galvanostat electrochemical workstation (Eco Chemie B. V, Netherlands) by using NOVA 10.1 software. The working electrode was a glassy carbon electrode (3 mm in diameter), on which 5 μL of an ink of the catalyst was applied. The ink [3 mg mL^{-1}] consisted of 30 μL Nafion® solution (5 wt%, Sigma–Aldrich solution) and 600 μL isopropyl alcohol. The counter and reference electrodes were a Pt coil wire and a hydrogen electrode prepared in the same solution (HESS). Cyclic voltammograms (CVs) were performed in 0.5 M H_2SO_4 (≥99.5%, Sigma–Aldrich) or 0.5 M KOH (≥99.5%, Sigma–Aldrich) from 25 to 65 °C between +0.05 and +1.3 V *versus* RHE (reversible hydrogen electrode) at $\nu = 20$ m V s^{-1}. For the measurements of ethanol electrooxidation activity, 0.5 M ethanol (High purity ≥99.999%, Sigma–Aldrich) were added into the supporting electrolyte. Before the experiments, N_2 gas was flowed over the solution to minimize the dissolved O_2 in solution. The CO stripping experiments were carried out by bubbled CO through the electrolyte at 0.1 V until complete blocking of the surface. N_2 was then bubbling for remove CO present in the solution. CO-stripping voltammograms were registered from 0.05 to +1.3 V *versus* RHE at 10 mV s^{-1}. The real surface area of the electrodes was estimated by calculating the charge from CO_{ads} stripping voltammograms (assuming 420 μC cm^{-2} for one CO monolayer) [34]. Temperature studies in CO_{ads} coverage on Ni@Pt/C nanoparticles were performed from 30 to 60 °C.

2.5. Temperature and activation energy studies

The ethanol electrooxidation was also studied using LSV at 10 mV s^{-1}. Besides, chronoamperometric experiments were carried out at different potentials (selected from linear scans in each electrolyte) for 200 s in the potentiostatic mode. Temperature-controlled LSV experiments were carried out to calculate the E_a of ethanol electrooxidation at different potentials. The pH of the electrolytes varied from pH = 2.0 in 0.5 M H_2SO_4 to pH = 14 in 0.5 M KOH. The temperature ranged from 25 to 65 °C. The E_a was calculated in the onset potential obtained by LSVs and data are analyzed using the Arrhenius Equation.

3. Results and discussion

3.1. Physico-chemical characterization

Fig. 1A and B show a TEM image and the corresponding size distribution histograms for the Ni@Pt/C catalyst. Core-shell Ni@Pt particles have an average diameter of 2.9 ± 0.4 nm and spherical shape. The XRD patterns are shown in Fig. 1C for Ni@Pt/C and Pt/C catalysts. The Ni@Pt/C catalyst exhibits a face-centered cubic (fcc) structure where the peaks are shifted to higher angles (41.7°, 48.1°, 69.6°, and 83.1°) from the respective peaks of Pt/C (39.8°, 46.3°, 67.2°, and 81.3). The slight shift of the XRD peaks toward higher 2θ values means a lattice compression of the Pt shell in the presence of Ni core as well as could indicate the formation of some NiPt alloyed nanoparticles. Considering the positions of the peaks presented, the lattice parameter, *a*, estimated was 3.83 Å for Ni@Pt/C, and 3.91 Å of Pt. This result suggests that the central Ni atoms induce compression of the Pt—Pt distance in the shell of Ni@Pt. No peaks corresponding to nickel oxide species were found in the Ni@Pt sample.

The elemental mapping in Fig. 1D and E reveal the presence of the Pt and Ni elements, which coincided with XRD data. The STEM-EDX spectrum (Fig. 1F) illustrate that the particles are composed of Pt and Ni with a composition of *ca.* 26.6 at.% Ni 73.4 at.% Pt. From these values, it is possible to establish that particulates of metals have 1:3, which is related with the larger atomic size of Pt than Ni [18], which can suggest that

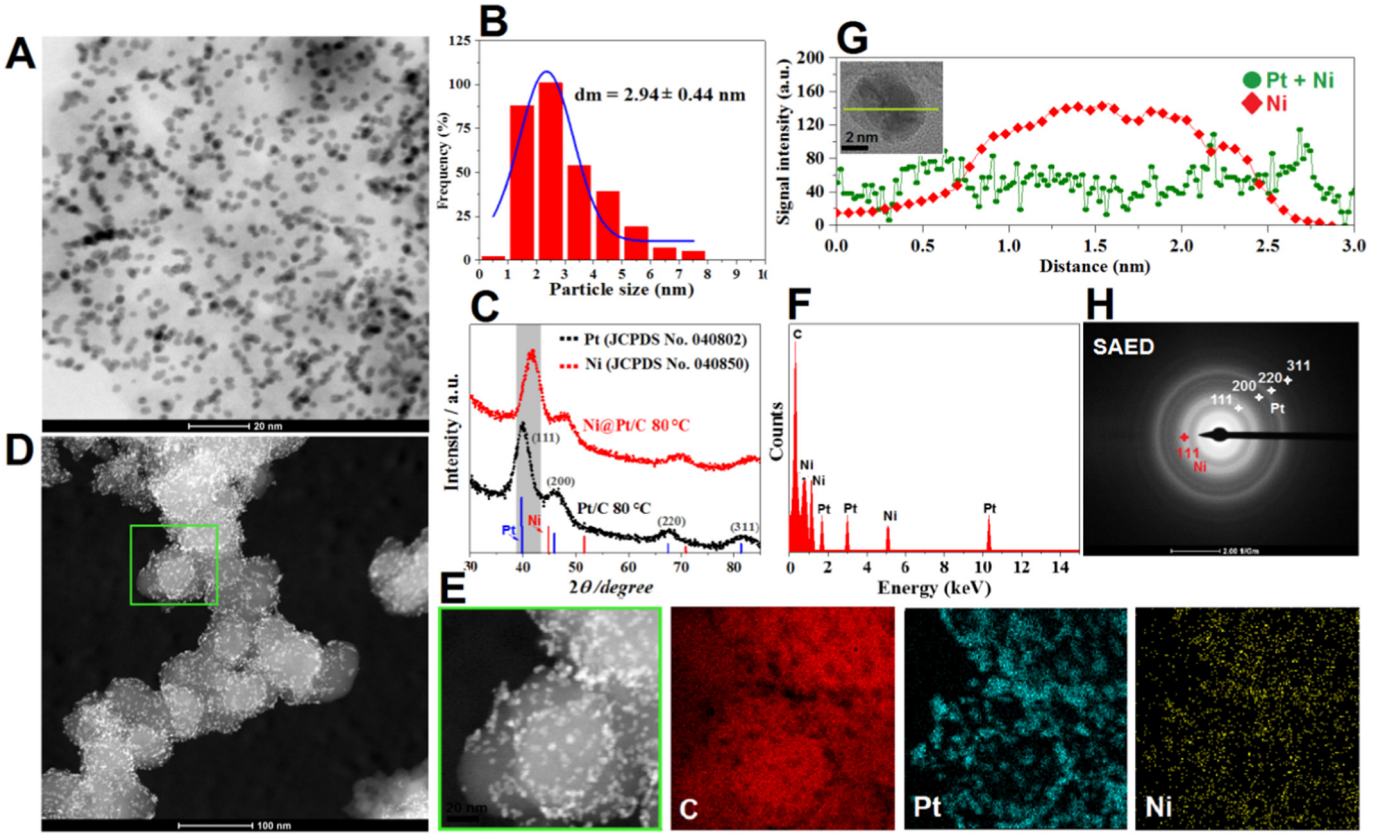

Fig. 1. Structural analysis results (A) TEM image and (B) respective size distribution histogram. (C) XRD patterns of the Ni@Pt/C and Pt/C samples and the positions of pure polycrystalline Pt and Ni. (D and E) TEM image and elemental maps. (F) EDX spectrum of the Ni@Pt/C catalysts, (G) Elemental line profiles taken in STEM mode across an individual ~5 nm diameter Ni@Pt particle nanoparticle shown in the HRTEM image in the inset top and (H) SAED pattern.

the Pt has been deposited on the surface of Ni seed particles. The elemental composition is close to the nominal (theoretical) catalyst composition (*i.e.*, 25 at.% Ni 75 at.% Pt).

The HRTEM image in the inset of Fig. 1G shows a contrast between a shell surrounding a darker core. The brightness contrast between regions could suggest the formation of core-shell nanoparticles. The HR-EDX line elemental profile of an arbitrarily chosen single-particle (inset of Fig. 1G) obtained in the STEM mode (Fig. 1G) reveal that the Pt signal is present throughout the particle whereas the Ni signal is more intense only in the core particle region, therefore, it could suggest a core-shell structure. Finally, Fig. 1H, taken from a large area containing NPs in Fig. 1D, shows the corresponding SAED pattern of Ni@Pt catalyst, revealing their polycrystalline nature. It was possible to identify four diffraction rings, indexed as the characteristic rings of Pt fcc structure, which is consistent with XRD data. Besides, the (111) diffraction ring of Ni confirms the presence of Ni in the catalyst.

3.2. Electrochemical characterization

3.2.1. Cyclic voltammetry in acid and alkaline solutions

Fig. S2 displays the CVs in 0.5 M H_2SO_4 treated by ethylene glycol–water solution before and after oxidized carbon Vulcan® XC-72R. The main feature shown in Fig. S2 is the redox couple at about 0.60 V and 0.55 V *versus* RHE (peaks I and II), which are only visible in the curve for the oxidized carbon. The increase in the electrochemical response of carbon after oxidation suggests that additional functional groups (*e.g.*, COOH and OH^-) were successfully introduced on the carbon surface through the acidic treatment [35,36]. The functionalities on the carbon surface in the form of surface oxides are responsible for both the acid/base and the redox properties of the carbon [37].

The CV curves of the Pt/C and Ni@Pt/C catalysts, both prepared 80 °C, are shown in Fig. 2. Fig. 2A and B shows that the hydrogen ad/desorption and oxide species formation/reduction regions of the Ni@Pt/C are similar to the one of Pt/C surface, implying that the surface of the nanoparticles is rich in Pt. It also suggests the formation of core–shell structures (Ni@Pt).

The EOR at Ni@Pt/C and Pt/C catalysts was measured by CVs, Fig. 2C, and D. The current densities are normalized by the electrochemical active area of the working electrode taken from CO stripping data discussed hereafter. The EOR onset potential in acid electrolyte shifts 60 mV to more negative potentials at the Ni@Pt/C catalyst related to Pt/C; consequently, the kinetic also is improved. Specifically, the Ni@Pt/C (80 °C) catalyst showed about 1.4 in H_2SO_4, and 1.3 in KOH fold higher peak current density than Pt/C.

The NiPt core–shell structure leads to a down-shift of the Pt 5*d*-band center produced by the interactions in the lattice of Pt atoms [38]. This phenomenon would result in weaker adsorption of some adsorbates such as CO or CH_x [39,40] on Pt atoms and, thus, in the acceleration of the CO electrooxidation kinetics on Ni@Pt/C.

3.2.2. CO-Stripping at high temperature

The effect of the CO_{ads} coverage on Ni@Pt/C in 0.5 M H_2SO_4 and 0.5 M KOH was studied by CO_{ads} stripping experiments at room temperature (Fig. 3A and B, respectively). The CO-stripping data were used to estimate the real surface area of the electrodes. The first anodic scan was performed to electrooxidize the CO adsorbed, and the subsequent voltammetry was done to verify the completeness of the CO oxidation. The onset and peak potential for CO-stripping occur in 710 and 820 mV *versus* RHE, at 25 °C, in acidic medium, as well as in 430 and 680 mV *versus* RHE in alkaline medium. Hence, the onset potential is 276 mV more negative in alkaline than in acidic medium. This behavior could be due

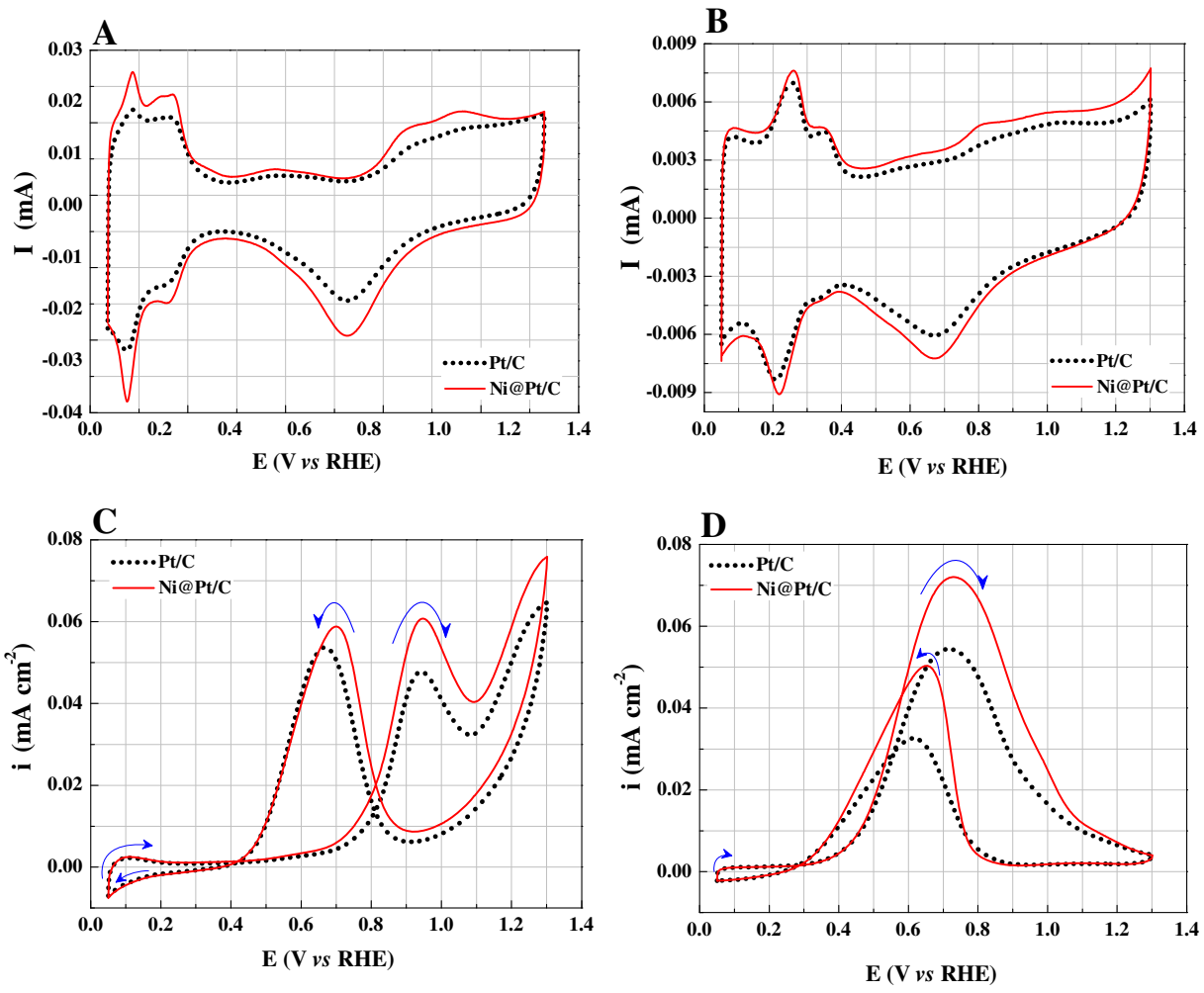

Fig. 2. Cyclic Voltammograms in (A) 0.5 M H_2SO_4, (B) 0.5 M KOH, (C) acid electrolyte +0.5 M ethanol and (D) basic electrolyte +0.5 M ethanol on Scan rate: 20 mV s^{-1}.

to in alkaline media, the specific adsorption of anions from de electrolyte almost no occurs, the free OH^- groups adsorb onto the surfaces of the catalysts, thus facilitating the oxide formation at lower potentials [41]. On the contrary, in acid solution at low overpotentials OH adsorbed is most likely excluded from active sites (*e.g.*, the dipole moment at defect/step sites which are intrinsically attractive to anions) [41]. The integrated CO stripping charges for the voltammograms in both media are 1740.45 μC and 1722.21 μC for 0.5 M H_2SO_4 and 0.5 M KOH, respectively.

Fig. 3C and D shows that the CO_{ads} oxidation peaks shift to more cathodic potentials, and the CO_{ads} coverage are variable with increasing temperature from 30 °C to 60 °C on both electrolytes. As a consequence: (*i*) it can be assumed that the increasing temperature destabilizes CO_{ads} species thus lowering the Pt–CO adsorption strength [42] or (*ii*) the more natural generation of OH_{ads}-species at higher temperature (enabling high electrocatalyst coverage of OH_{ads} species at low potentials) could also facilitate the CO_{ads} electrooxidation at lower potentials [43–45]. The CO-stripping onset potentials are lower for alkaline (540–620 mV *versus* RHE, inset Fig. 3D) than acid electrolyte (660–780 mV, inset Fig. 3C). Furthermore, in the range 30–60 °C, the peak current decreases 94 μA for KOH and increases 120 μA for H_2SO_4 (insets in Fig. 3C and D).

3.2.3. Potentiodynamic experiments at different temperatures

Cyclic voltammetry experiments were carried out at different temperatures (25–65 °C) in H_2SO_4 and KOH electrolytes (Fig. S3). This temperature range was chosen due to the low boiling point of ethanol (78 °C). The voltammetric profiles remain almost unchanged as the temperature is increased from 25 to 65 °C [46,47]; however, the profiles are better-defined at the highest temperature. Kita et al. [48] pointed out that the adsorption of oxygenated species does not affect the surface structure. The formation of metal oxides and water dissociation ($H_2O \leftrightarrow H^+ + OH^-$) are slightly improved when the temperature increases from 25 to 65 °C. In the negative scan, the current of the oxide reduction increases as the temperature increases and the peak potential, E_{peak}, shifts slightly toward positive potentials, mainly in alkaline medium. The positive shift results from the lower stability of the oxides at the catalyst surface when the temperature increases.

Hydrogen ad/desorption peaks are more intense with increasing temperatures (Fig. 4A). The increase in oxide coverage also depends on the pH of the electrolyte [46,49]. In the H_2SO_4 solution, the oxide reduction charge increases by 23% (Fig. 4A) as the temperature increases from 20 to 65 °C.

Fig. 4B shows the integrated charge density *vs* temperature for the oxide reduction peak ($q_{PtO-red}$). The charge density increases linearly with temperature increase within the temperature range studied (20–65 °C). The slope of the line is *ca.* 2.5 μC cm^{-2} $°C^{-1}$. This increase in oxide reduction charge at the Ni@Pt/C catalyst suggests that the higher the temperature, the higher the adsorption of OH^- on the metal surface caused by compressive-strain effects probably [18]. This feature needs to be considered when temperature-dependent experiments are carried out in the presence of OH^- that can react during the overall alcohol oxidation, thus aiding the oxidation of poisonous intermediate species, such as CO.

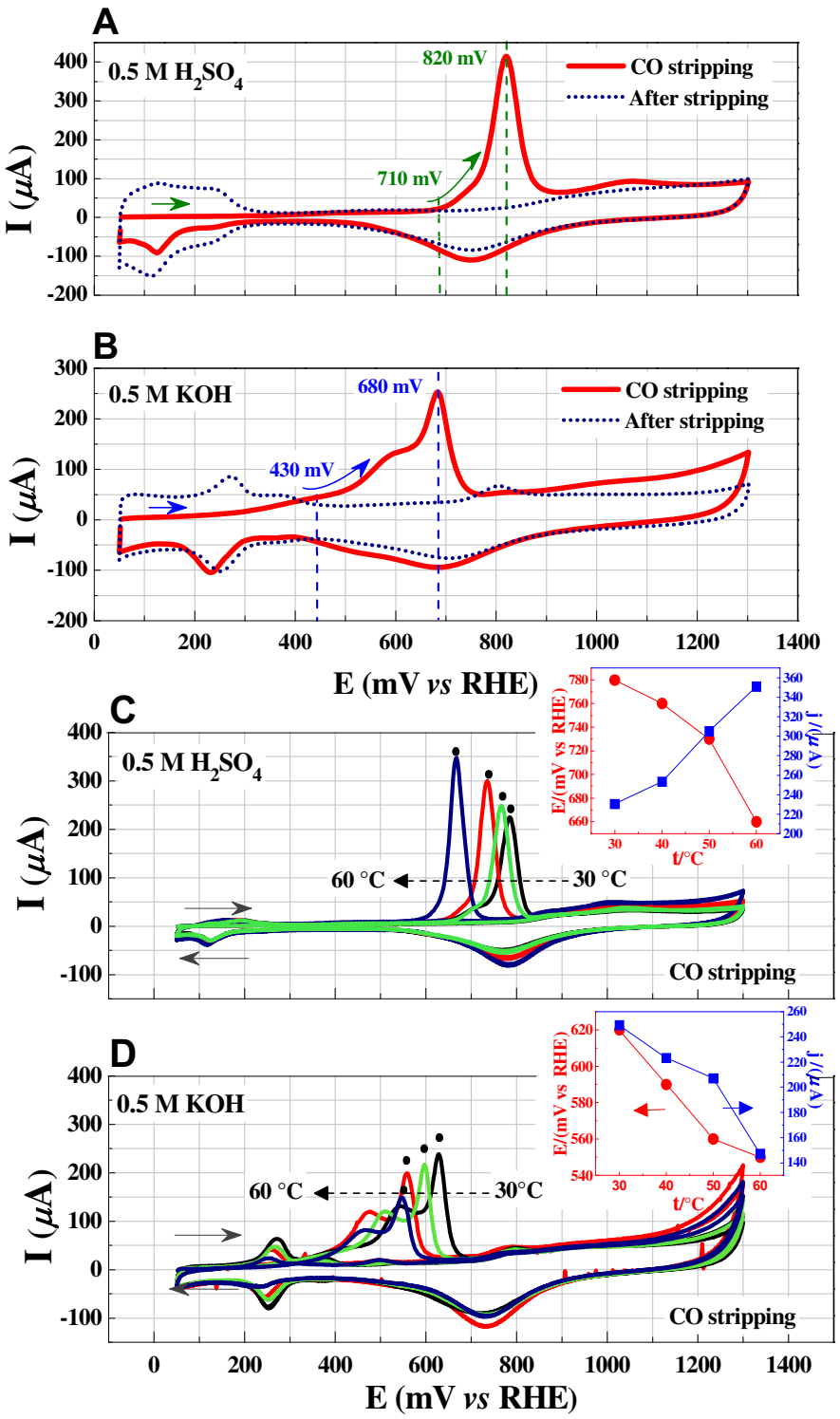

Fig. 3. CO_{chem} stripping voltammograms for Ni@Pt/C electrode after CO adsorption from CO-saturated for 25 min (full line) at room temperature in (A) 0.5 M H_2SO_4 and (B) 0.5 M KOH. Voltammetric profiles after CO stripping (dashed line). CO-stripping at different temperatures (T: 30, 40, 50 and 60 °C) for both solutions (C) 0.5 M H_2SO_4 and (D) 0.5 M KOH solutions. Scan rate 10 mV s^{-1}.

The cyclic voltammograms can be used as fingerprints of Ni@Pt/C electrode because the hydrogen and anion ad/desorption are structure-sensitive on Pt surfaces. Previous reports [50–52] show that anions adsorption can inhibit the formation of superficial Pt oxides in acidic media. Thus, free OH^- groups adsorb to the Pt surface, facilitating oxide formation, because anion adsorption in alkaline media is very low [50,52]. Here, the oxide reduction charge for $q_{PtO-red}$ = 0.2 μC cm^{-2} $°C^{-1}$ increases 6.78% in the alkaline electrolyte, when the temperature increases from 25 to 65 °C (Table 1).

As already observed by Alsabet et al. [47] at Pt electrodes, the increase in the oxide reduction peak sharpness is associated with enhancements in the attractive surface interactions between the adsorbed oxide species when the temperature increases, thus leading to increased kinetics [53]. Fig. 4C plots the E_{peak} (mV) of the Ni@Pt/C

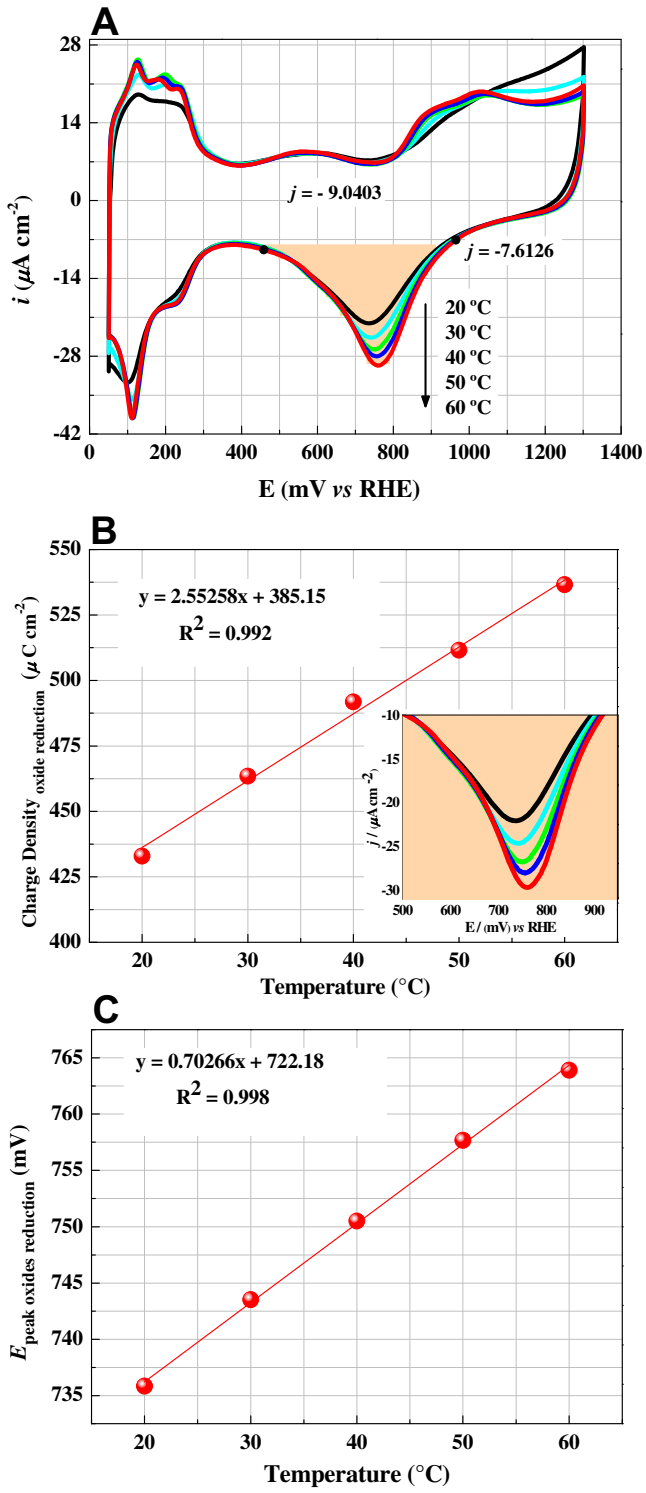

Fig. 4. (A) Cyclic voltammograms of Ni@Pt/C electrode in 0.5 M H_2SO_4 within the temperature range of 20–60 °C, $\nu = 20$ mV s^{-1}; (B) Oxide reduction charge (μC) *vs* electrolyte temperature (°C) for Ni@Pt/C electrode and zoom of the oxide reduction peak (inset below); (C) Peak potential (E_{peak}) for the Ni@Pt/C electrode oxide reduction *vs* electrolyte temperature (°C). Data were obtained from the cyclic voltammograms in Fig. 4A.

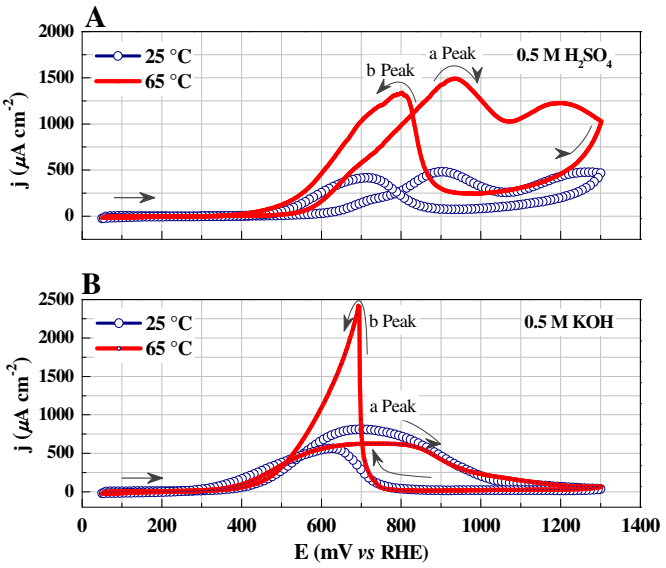

Fig. 5. Cyclic voltammograms in the presence of 0.5 M ethanol for Ni@Pt/C electrode in (A) 0.5 M H_2SO_4 and (B) 0.5 M KOH electrolyte at different electrolyte temperatures. $\nu = 20$ mV s^{-1}.

oxide reduction *versus* temperature (K) in 0.5 M H_2SO_4 electrolyte. The linear slope of this plot predicts a potential shift of +0.70 mV $°C^{-1}$ for the reduction of the Pt surface oxide in this temperature range (Table 1). Furthermore, data in Table 1 also show that for the alkaline electrolyte, an even more significant change with temperature is seen (+0.85 mV $°C^{-1}$).

Fig. 5 displays the cyclic voltammograms of ethanol oxidation on Ni@Pt/C at 25 and 65 °C in acidic and alkaline media. The ethanol adsorption inhibits the hydrogen ad/desorption and the two waves commonly observed for ethanol oxidation are observed in both media and temperatures. In an acid electrolyte at higher temperature, the peak current density and the onset potential of ethanol oxidation shifts negatively. While the current density of the forward peak increases 3-folds for H_2SO_4, the same decreases by a factor of 1.3 for KOH as the temperature increases from 25 °C to 65 °C. Nevertheless, the ethanol re-oxidation peak (≪*b*≫) increases around 3-fold at KOH electrolyte as the temperature increases, probably due to differences in the formation and dissolution of oxides as the temperature changes during EOR. Batista et al. [54] attributed this hysteresis to differences in surface oxide coverage on the anodic and cathodic voltammetric scans.

Since the re-oxidation peak is related to the reduction of adsorbed OH^- [40], its pronounced increase suggests that the reduction of adsorbed OH^- occurs quickly at high temperature on Ni@Pt/C (in the alkaline electrolyte). Furthermore, the difference between the oxidation and re-oxidation peaks intensity in KOH electrolyte is associated with poisonous intermediates adsorbed onto the catalyst electrode surface at low potentials [40], thus varying the nature of its surface due to the ease dissolution of OH^- species on the Ni@Pt/C surface. As previously observed, the most considerable shift (+0.85 mV $°C^{-1}$) of the oxide reduction peak with the temperature was found in 0.5 M KOH (Fig. S3B). This behavior is prevalent in Ni@Pt systems [18,19].

The temperature plays a significant role in the EOR performances in acidic and alkaline media. Behm et al. [55] suggested that temperature is the main parameter affecting the C—C bond breaking during ethanol

Table 1
Dependence of the Pt oxide reduction peak parameters with the electrolyte temperature in acidic and alkaline media.

Electrolyte/temperature interval	Charge/μC cm^{-2} $°C^{-1}$	% Pt oxide charge increase	Oxide reduction peak potential shift/mV $°C^{-1}$
0.5 M H_2SO_4, (20°–60 °C)	2.5	23.93	+0.70
0.5 M KOH, (25°–65 °C)	0.2	6.78	+0.85

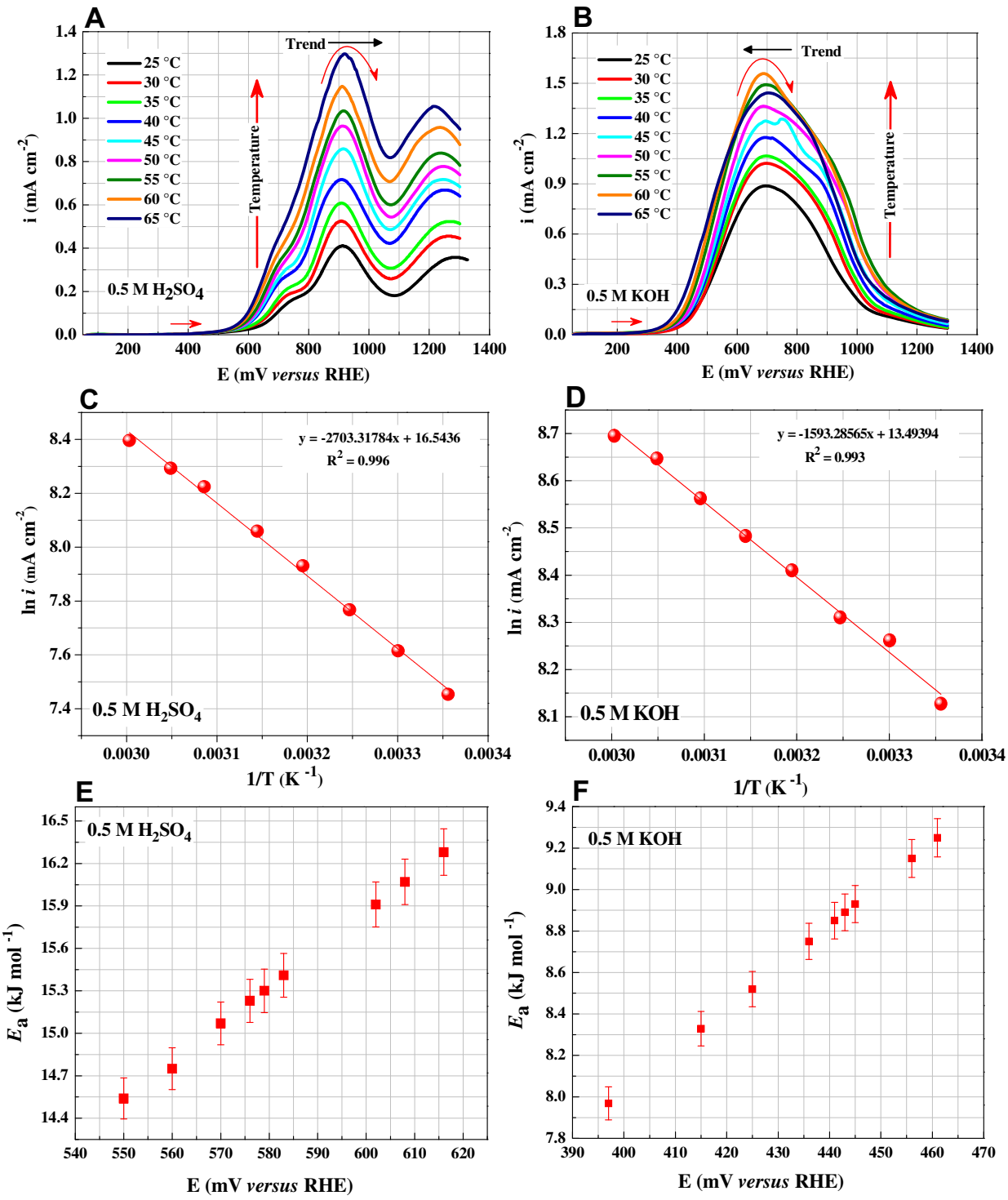

Fig. 6. (A and B) linear sweep voltammetry of Ni@Pt/C at different temperatures ($\nu = 10$ mV s^{-1}); (C and D) Arrhenius plots and (E and F) activation energies as a function of electrode potential for 0.5 M ethanol in (A) 0.5 M H_2SO_4 and (B) 0.5 M KOH, respectively.

electrooxidation. Presumably, CO affinity on the Ni@Pt/C is reduced with temperature increase, as discussed in the CO-stripping section. The lower EOR onset potential at the Ni@Pt/C in KOH than in H_2SO_4 electrolyte is associated with the anions adsorption on the catalyst surface that can block surface sites preventing alcohol adsorption in the acid medium [11,46,51,52].

The EOR onset potential, in an acidic electrolyte, shifts negatively around 90 mV with the increase in temperature, while it is unchanged in the alkaline electrolyte (Fig. 5A). The adsorption of anions is disfavored as the temperature increases [56] on the platinum surfaces in H_2SO_4, followed by the enhancement of ethanol adsorption at low potentials [57] and by an enhancement in the dehydrogenation until acetaldehyde [31].

Another temperature effect that should be highlighted is the potential peak shift of «*a*» and «*b*» peaks (Fig. 5). These peaks move positively with temperature increase. Since those peaks are strongly related to OH^- production by H_2O dissociation [26], the potential difference suggests that OH^- production on Ni@Pt/C is activated at a higher temperature. Considering that the oxidative desorption of CO_{ads} requires the presence of species containing oxygen [49], this is a positive

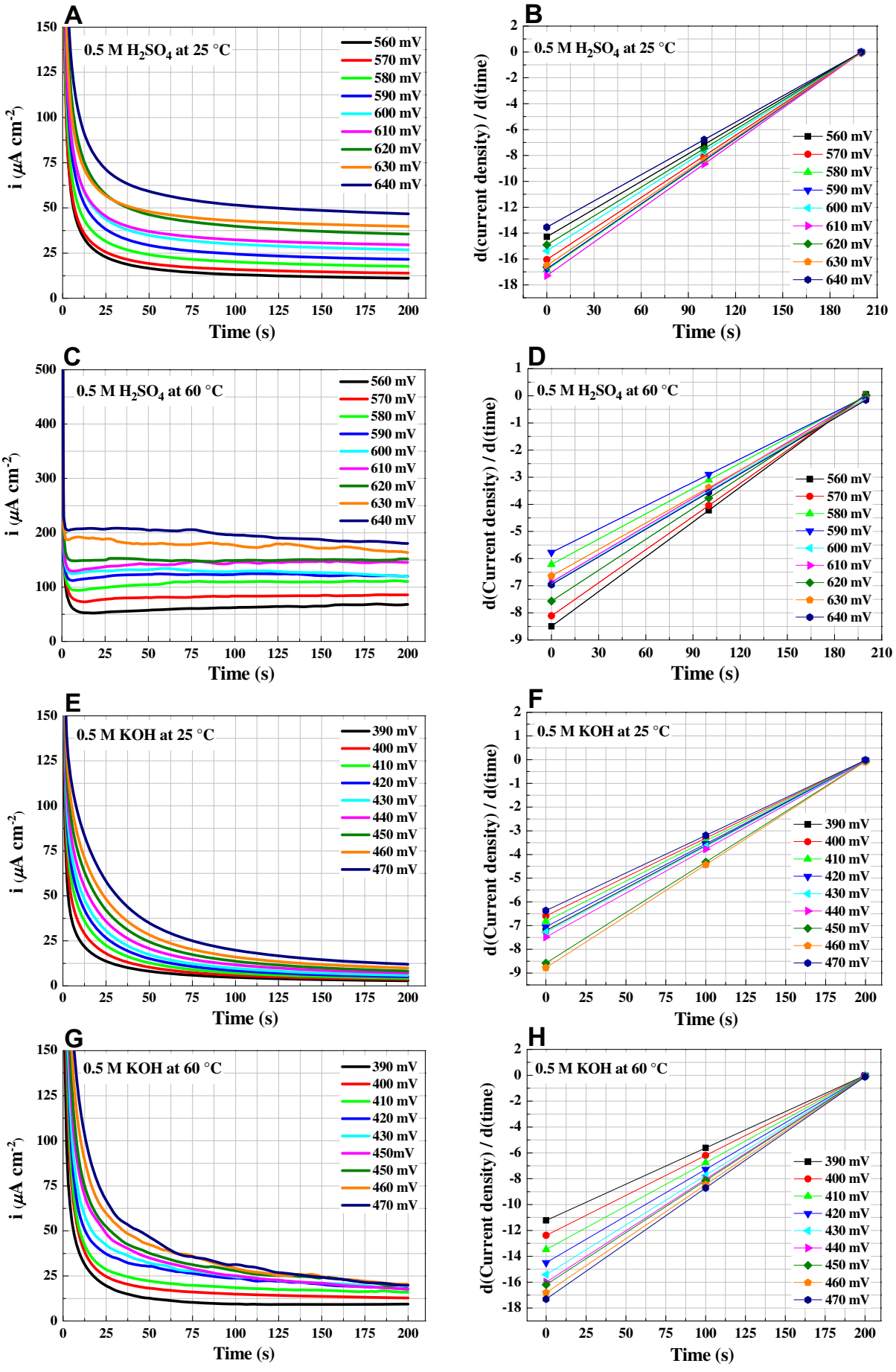
A
0.5 M H2SO4 at 25 °C
560 mV
570 mV
580 mV
590 mV
600 mV
610 mV
620 mV
630 mV
640 mV
i (μA cm-2)
Time (s)
B
0.5 M H2SO4 at 25 °C
d(current density) / d(time)
Time (s)
C
0.5 M H2SO4 at 60 °C
i (μA cm-2)
Time (s)
D
0.5 M H2SO4 at 60 °C
d(Current density) / d(time)
Time (s)
E
0.5 M KOH at 25 °C
390 mV
400 mV
410 mV
420 mV
430 mV
440 mV
450 mV
460 mV
470 mV
i (μA cm-2)
Time (s)
F
0.5 M KOH at 25 °C
d(Current density) / d(time)
Time (s)
G
0.5 M KOH at 60 °C
450mV
i (μA cm-2)
Time (s)
H
0.5 M KOH at 60 °C
d(Current density) / d(time)
Time (s)

result. Besides, the modification of Pt electronic structure induced by the presence of nickel in the lattice, as discussed for CO-stripping data, can reduce the Pt CO-adsorption affinity in 0.5 M H_2SO_4 at 65 °C.

3.3. Electrochemical measurements by linear voltammetry

3.3.1. Potentiodynamic experiments for ethanol oxidation

Fig. 6 displays the influence of the temperature (25–65 °C) on the specific activity toward EOR at the Ni@Pt/C catalyst in both media. E_a values are obtained from these data. In the acidic medium (Fig. 6A), the temperature increase leading to $E_{peak,ox}$ shifts to more positive potentials (*i.e.*, at 65 °C is 920 mV, and at 25 °C it is 912 mV). This positive potential shift is ascribed to the facilitated OH adsorption on Pt with the water decomposition at high temperatures as having been reported by Cohen et al. [53] and Sieben et al. [25]. In contrast, the potential for ethanol electrooxidation in KOH (Fig. 6B) shifts direction negatively with the increase from 25 to 60 °C (8 mV). Jiang et al. [46] also observed similar negative shifts associated with a higher affinity of OH^- for the catalyst surface in alkaline media, thus leading to a low onset of the formation of surface oxides. Our results confirm that the OH_{ads} species required for the removal of adsorbed ethoxy residues are more available in alkaline media.

Furthermore, the increase of temperature produces a negative shift in the onset potential and larger oxidation current densities because of the higher temperature, the higher the kinetics of the EOR. According to Delpeuch et al. [39], the down-shift of the onset potential and larger oxidation currents at high temperatures are ascribed to the C—C bond scission that becomes easier due to thermal activation and a smaller formation of incomplete oxidation byproducts (*e.g.*, CH_3CHO, CH_2CH_2COOH and especially CO). However, the current decays in KOH at 65 °C probably related to the easy desorption of OH^- species at temperatures above 60 °C. Consequently, the higher stability of CO superficial species onto Ni@Pt/C nanoparticles is observed (previously confirmed in CO stripping), preventing alcohol adsorption and therefore decreasing of the peak current.

Table S1 summarizes the E_a values determined by plotting data in Fig. 6 (ln (current (μA)) as a function of 1/T (K^{-1}) at a given potential). Fig. 6C and D shows the representative Arrhenius plots for EOR taken in both, 0.5 M H_2SO_4 and 0.5 M KOH medium, respectively. The slope, intercept, and *R*-values of the linear fits are also displayed on each graph.

Fig. 6E and F shows that the apparent E_a for the EOR using the Ni@Pt/C catalyst decrease from 16.28 to 14.54 kJ mol^{-1} in 0.5 M H_2SO_4 and from 9.25 to 7.97 kJ mol^{-1} in 0.5 M KOH when the temperature rises from 25 to 65 °C, respectively, as a function of the potential at which these E_a values were obtained. The relation between the apparent E_a and the potential has been already reported [28,30,31]. Colmati et al. [28] attributed the adsorption of ethanol on a Pt_3Sn/C electrode surface as the rate-determining step of the reaction.

The time-dependent surface coverage changes in both alkaline and acid electrolytes were also analyzed. Fig. 7 shows chronoamperometry data and the evaluation of the initial poisoning rate using $di/dt = f(t)$ plot (normalized scale) at 200 s, with values obtained from experiments carried out at 25 and 65 °C. The tests were carried out at 9 different potentials that considering the range of onset potential observed for ethanol oxidation by LSV in each electrolyte.

In acidic media, at 25 °C, the currents decay with time and reach an apparent steady state within 200 s (Fig. 7A). Nevertheless, at 65 °C, after a significant initial decay, the current attains the quasi-steady status mainly at high potentials (Fig. 7A) [58]. This observation is confirmed from Fig. 7B and D that present $di/dt = f(t)$ plot *versus* time. The higher the slope, the easier the initial poisoning of the electrode surface. The slopes are in the range 0.07–0.09 at 25 °C and in the range of 0.03–0.04 at 60 °C. Therefore, the steady-state current density is attained much earlier at 60 °C than at 25 °C, reflecting favorable ad/desorption kinetics at high temperature in 0.5 M H_2SO_4.

In contrast, in Fig. 7E and G, the current density continuously decays during the 200 s of the experiment for the two temperatures (25 and 60 °C) in 0.5 M KOH. Besides, low current densities are observed at 60 °C. This fact is attributed to the smaller tolerance to ethanolic residues when the electrolyte reaches 60 °C. The adsorbed intermediates inhibit further oxidation of alcohol [27].

Fig. 7F and H shows the slopes between 0.03 and 0.04 and 0.06–0.09 take at 25 and 60 °C, respectively. The increased inclination at 60 °C may be related to the difficulty of attainment the adsorption-desorption alcohol equilibrium. In alkaline media, Shen et al. [59] reported that the EOR performance depends on the local concentration ns of ethanol and OH^- ions as well as on the balance of the competing adsorption between ethanol and the OH_{ads} species. The results are like those of CV and LSV data at temperatures above 60 °C in alkaline electrolyte.

Fig. S4 shows the poisoning rates (% δ) in each electrolyte determined from chronoamperometric measurements as described by Datta et al. [27]. The Ni@Pt/C catalyst exhibits improved tolerance to ethanolic residues poisoning in the acid electrolyte and at high temperatures (60 °C).

4. Conclusions

In this study, Ni@Pt catalysts supported on functionalized carbon were synthesized to evaluate the effect of both acidic and alkaline media and working temperature (25–65 °C) on the kinetics of the EOR. The Ni@Pt nanoparticles exhibit a significantly enhanced electrochemical activity toward the EOR. Furthermore, the CO_{ads} oxidation to CO_2 is inhibited, and the kinetics of the alcohol oxidation is decreased during the ethanol oxidation at higher temperatures (around 60 °C) in alkaline media. Instead, the onset potentials of the ethanol oxidation reaction shift negatively with the temperature increase in acidic electrolytes. Moreover, in an acidic electrolyte, the increase in the temperature improved the electrocatalytic activity toward ethanol oxidation, by reducing the activation energies and the charge-transfer resistances. The data obtained in elevated temperatures can allow identifying parameters of operation that have an influence on the electrocatalytic properties of ethanol oxidation at a given potential to design efficient electrocatalysts to be used in DEFCs.

CRediT author statement

Lays S. R. Silva: Acquisition, analysis and interpretation of the data, Methodology, Investigation, Writing - Original Draft.

Iasmim G. Melo: Acquisition, analysis and interpretation of the data, validation, investigation.

Cristiano T. Meneses: Resources, Formal analysis, Writing - Review & Editing.

Franz E. Lopez-Suarez: Writing - Review & Editing, Visualization, Conceptualization.

Katlin I. B. Eguiluz: Project administration, Supervision, Funding acquisition, conceptualization and planning of the work and Writing - Review & Editing.

Giancarlo R. Salazar-Banda: Project administration, Supervision, Funding acquisition, conceptualization and planning of the work and Writing - Review & Editing.

Declaration of competing interest

The authors declare that they have no known competing financial interests or personal relationships that could have appeared to influence the work reported in this paper.

Fig. 7. Chronoamperometry and d*i*/d*t* (normalized scale) against *t* plots from $t = 0$ to $t = 200$ s for the Ni@Pt/C catalyst at different temperatures; (A and B) at 25 °C and (C and D) at 60 °C of 0.5 M ethanol in 0.5 M H_2SO_4, (E and F) at 25 °C and (G and H) at 60 °C of 0.5 M ethanol in 0.5 M KOH, respectively.

Acknowledgments

The authors would like to thank the CNPq (grant nos. 407274/2013-8, 400443/2013-9, 407286/2016-0, 402243/2012-9, 304419/2015-0, 305438/2018-2, and 310282/2013-6), to CAPES (Grant: 001), and to FAPITEC/SE from Brazil, for financial support and scholarships.

Appendix A. Supplementary data

Supplementary data to this article can be found online at https://doi.org/10.1016/j.jelechem.2019.113754.

References

[1] M.S. Dresselhaus, I.L. Thomas, Alternative energy technologies, dresselhaus2001 Nature 414 (2001) 332–337, https://doi.org/10.1038/35104599.
[2] G.W. Huber, S. Iborra, A. Corma, Synthesis of transportation fuels from biomass: chemistry, catalysts, and engineering, Chem. Rev. 106 (2006) 4044–4098, https://doi.org/10.1021/cr068360d.
[3] M. Miller, A. Bazylak, A review of polymer electrolyte membrane fuel cell stack testing, J. Power Sources 196 (2011) 601–613, https://doi.org/10.1016/j.jpowsour.2010.07.072.
[4] M.Z.F. Kamarudin, S.K. Kamarudin, M.S. Masdar, W.R.W. Daud, Review: direct ethanol fuel cells, Int. J. Hydrog. Energy 38 (2013) 9438–9453, https://doi.org/10.1016/j.ijhydene.2012.07.059.
[5] A.M. Sheikh, K.E.-A. Abd-Alftah, C.F. Malfatti, On reviewing the catalyst materials for direct alcohol fuel cells (DAFCs), Energy 1 (2014) 1–10.
[6] A. Brouzgou, A. Podias, P. Tsiakaras, PEMFCs and AEMFCs directly fed with ethanol: a current status comparative review, J. Appl. Electrochem. 43 (2013) 119–136, https://doi.org/10.1007/s10800-012-0513-2.
[7] H. Wang, Z. Jusys, R.J. Behm, H.D. Abruña, New insights into the mechanism and kinetics of adsorbed CO electrooxidation on platinum: online mass spectrometry and kinetic Monte Carlo simulation studies, J. Phys. Chem. C 116 (2012) 11040–11053, https://doi.org/10.1021/jp301292p.
[8] J. Chang, L. Feng, C. Liu, W. Xing, X. Hu, Ni2P enhances the activity and durability of the Pt anode catalyst in direct methanol fuel cells, Energy Environ. Sci. 7 (2014) 1628–1632, https://doi.org/10.1039/c4ee00100a.
[9] M.H. Shao, J. Warren, N.S. Marinkovic, P.W. Faguy, R.R. Adzic, In situ ATR-SEIRAS study of electrooxidation of dimethyl ether on a Pt electrode in acid solutions, Electrochem. Commun. 7 (2005) 459–465, https://doi.org/10.1016/j.elecom.2005.02.024.
[10] D. Bayer, S. Berenger, C. Cremers, J. Tübke, Concentration dependence of the electrooxidation of ethanol and ethylene glycol at platinum in alkaline medium, ECS Trans. 25 (2010) 95–103, https://doi.org/10.1149/1.3315176.
[11] S.C.S. Lai, S.E.F. Kleijn, F.T.Z. Öztürk, V.C. Van Rees Vellinga, J. Koning, P. Rodriguez, et al., Effects of electrolyte pH and composition on the ethanol electro-oxidation reaction, Catal. Today 154 (2010) 92–104, https://doi.org/10.1016/j.cattod.2010.01.060.
[12] C.V.S. Almeida, D.S. Ferreira, H. Huang, A.C. Gaiotti, G.A. Camara, A.E. Russell, et al., Highly active Pt3Rh/C nanoparticles towards ethanol electrooxidation. Influence of the catalyst structure, Appl. Catal. B Environ. 254 (2019) 113–127, https://doi.org/10.1016/j.apcatb.2019.04.078.
[13] G.R. Salazar-Banda, H.B. Suffredini, L.A. Avaca, Improved stability of PtOx sol-gel-modified diamond electrodes covered with a Nafion® film, J. Braz. Chem. Soc. 16 (2005) 903–906, https://doi.org/10.1590/S0103-50532005000600003.
[14] H. Huang, X. Wang, Recent progress on carbon-based support materials for electrocatalysts of direct methanol fuel cells, J. Mater. Chem. A 2 (2014) 6266–6291, https://doi.org/10.1039/c3ta14754a.
[15] D.F. Van Der Vliet, C. Wang, D. Tripkovic, D. Strmcnik, X.F. Zhang, M.K. Debe, et al., Mesostructured thin films as electrocatalysts with tunable composition and surface morphology, Nat. Mater. 11 (2012) 1051–1058, https://doi.org/10.1038/nmat3457.
[16] D.F. Van Der Vliet, C. Wang, D. Li, A.P. Paulikas, J. Greeley, R.B. Rankin, et al., Unique electrochemical adsorption properties of Pt-skin surfaces, Angew. Chem. Int. Ed. 51 (2012) 3139–3142, https://doi.org/10.1002/anie.201107668.
[17] L.S.R. Silva, F.E. López-Suárez, M. Perez-Cadenas, S.F. Santos, L.P. da Costa, K.I.B. Eguiluz, et al., Synthesis and characterization of highly active Pb x @Pt y/C core-shell nanoparticles toward glycerol electrooxidation, Appl. Catal. B Environ. 198 (2016) 38–48, https://doi.org/10.1016/j.apcatb.2016.04.046.
[18] Y. Chen, F. Yang, Y. Dai, W. Wang, S. Chen, Ni@ Pt core—shell nanoparticles: synthesis, structural and electrochemical properties, J. Phys. Chem. C 112 (2008) 1645–1649.
[19] Y. Chen, Z. Liang, F. Yang, Y. Liu, S. Chen, Ni-Pt core-shell nanoparticles as oxygen reduction electrocatalysts: effect of Pt shell coverage, J. Phys. Chem. C 115 (2011) 24073–24079, https://doi.org/10.1021/jp207828n.
[20] H. Ogasawara, C. Yu, Z. Liu, S. Koh, P. Strasser, S. Kaya, et al., Lattice-strain control of the activity in dealloyed core–shell fuel cell catalysts, Nat. Chem. 2 (2010) 454–460, https://doi.org/10.1038/nchem.623.
[21] L. Gan, C. Cui, M. Heggen, F. Dionigi, S. Rudi, P. Strasser, Element-specific anisotropic growth of shaped platinum alloy nanocrystals, Science 346 (2014) 1502–1506, https://doi.org/10.1126/science.1261212.
[22] W. Yu, M.D. Porosoff, J.G. Chen, ChemInform abstract: review of Pt-based bimetallic catalysis: from model surfaces to supported catalysts, ChemInform 44 (2013) https://doi.org/10.1002/chin.201306180no-no.
[23] S. Mukerjee, Particle size and structural effects in platinum electrocatalysis, J. Appl. Electrochem. 20 (1990) 537–548, https://doi.org/10.1007/BF01008861.
[24] S. Wang, Sheets toward oxygen reduction reaction electrocatalytic activity of Co_3O_4 anchored on graphene sheets toward, Sci. Rep. 3 (2013) 2300, https://doi.org/10.1038/srep02300.
[25] J.M. Sieben, M.M.E. Duarte, C.E. Mayer, Supported Pt and Pt-Ru catalysts prepared by potentiostatic electrodeposition for methanol electrooxidation, J. Appl. Electrochem. 38 (2008) 483–490, https://doi.org/10.1007/s10800-007-9462-6.
[26] C.G. Lee, M. Umeda, I. Uchida, Cyclic voltammetric analysis of C1-C4 alcohol electrooxidations with Pt/C and Pt-Ru/C microporous electrodes, J. Power Sources 160 (2006) 78–89, https://doi.org/10.1016/j.jpowsour.2006.01.068.
[27] J. Datta, A. Dutta, S. Mukherjee, The beneficial role of the cometals Pd and Au in the carbon-supported PtPdAu catalyst toward promoting ethanol oxidation kinetics in alkaline fuel cells: temperature effect and reaction mechanism, J. Phys. Chem. C 115 (2011) 15324–15334, https://doi.org/10.1021/jp200318m.
[28] F. Colmati, E. Antolini, E.R. Gonzalez, Effect of temperature on the mechanism of ethanol oxidation on carbon supported Pt, PtRu and Pt3Sn electrocatalysts, J. Power Sources 157 (2006) 98–103, https://doi.org/10.1016/j.jpowsour.2005.07.087.
[29] L.S. Foster, in: H.H. Uhlig (Ed.), Corrosion and Corrosion Control: An Introduction to Corrosion Science and Engineering, 41, John Wiley & Sons, 2009https://doi.org/10.1021/ed041pa126.5.
[30] A.F.B. Barbosa, V.L. Oliveira, J. Van Drunen, G. Tremiliosi-Filho, Ethanol electrooxidation reaction using a polycrystalline nickel electrode in alkaline media: temperature influence and reaction mechanism, J. Electroanal. Chem. 746 (2015) 31–38, https://doi.org/10.1016/j.jelechem.2015.03.024.
[31] A. Bach Delpeuch, T. Asset, M. Chatenet, C. Cremers, Influence of the temperature for the ethanol oxidation reaction (EOR) on Pt/C, Pt-Rh/C and Pt-Rh-SnO_2/C, Fuel Cells 15 (2015) 352–360, https://doi.org/10.1002/fuce.201400144.
[32] H. Lv, L. Sun, D. Xu, S.L. Suib, B. Liu, One-pot aqueous synthesis of ultrathin trimetallic PdPtCu nanosheets for the electrooxidation of alcohols, Green Chem. 21 (2019) 2367–2374, https://doi.org/10.1039/c9gc00741e.
[33] Y. Xing, Synthesis and electrochemical characterization of uniformly-dispersed high loading Pt nanoparticles on sonochemically-treated carbon nanotubes, J. Phys. Chem. B 108 (2004) 19255–19259, https://doi.org/10.1021/jp046697i.
[34] J.P. Iúdice De Souza, T. Iwasita, F.C. Nart, W. Vielstich, Performance evaluation of porous electrocatalysts via normalization of the active surface, J. Appl. Electrochem. 30 (2000) 43–48, https://doi.org/10.1023/A:1003896604569.
[35] W. Zhang, J. Chen, G.F. Swiegers, Z.F. Ma, G.G. Wallace, Microwave-assisted synthesis of Pt/CNT nanocomposite electrocatalysts for PEM fuel cells, Nanoscale 2 (2010) 282–286, https://doi.org/10.1039/b9nr00140a.
[36] B. Wu, J. Zhu, X. Li, X. Wang, J. Chu, S. Xiong, PtRu nanoparticles supported on p-phenylenediamine-functionalized multiwalled carbon nanotubes: enhanced activity and stability for methanol oxidation, Ionics 25 (2019) 181–189, https://doi.org/10.1007/s11581-018-2590-7.
[37] B. Harrison, Carbons as supports for precious metal catalysts, Catal. Today 7 (1990) 113–137, https://doi.org/10.1016/0920-5861(90)85012-D.
[38] S. Praserthdam, P.B. Balbuena, Effects of oxygen coverage, catalyst size, and core composition on Pt-alloy core-shell nanoparticles for oxygen reduction reaction, Catal. Sci. Technol. 6 (2016) 5168–5177, https://doi.org/10.1039/c5cy02287h.
[39] A. Bach Delpeuch, M. Chatenet, M.S. Rau, C. Cremers, Influence of H- and OH-adsorbates on the ethanol oxidation reaction - a DEMS study, Phys. Chem. Chem. Phys. 17 (2015) 10881–10893, https://doi.org/10.1039/c5cp00132c.
[40] J.F.E. Gootzen, W. Visscher, J.A.R. van Veen, Characterization of ethanol and 1,2-ethanediol adsorbates on platinized platinum with Fourier transform infrared spectroscopy and differential electrochemical mass spectrometry, Langmuir 12 (2002) 5076–5082, https://doi.org/10.1021/la960103o.
[41] N.M. Marković, C.A. Lucas, A. Rodes, V. Stamenković, P.N. Ross, Surface electrochemistry of CO on Pt(1 1 1): anion effects, Surf. Sci. 499 (2002) 149–158, https://doi.org/10.1016/S0039-6028(01)01821-0.
[42] E. Herrero, J.M. Feliu, S. Blais, Z. Radovic-Hrapovic, G. Jerkiewicz, Temperature dependence of CO chemisorption and its oxidative desorption on the Pt(111) electrode, Langmuir 16 (2000) 4779–4783, https://doi.org/10.1021/la9907432.
[43] P.P. Lopes, K.S. Freitas, E.A. Ticianelli, CO tolerance of PEMFC anodes: mechanisms and electrode designs, Electrocatalysis 1 (2010) 200–212, https://doi.org/10.1007/s12678-010-0025-y.
[44] A.R. Kucernak, G.J. Offer, The role of adsorbed hydroxyl species in the electrocatalytic carbon monoxide oxidation reaction on platinum, Phys. Chem. Chem. Phys. 10 (2008) 3699–3711, https://doi.org/10.1039/b802816h.
[45] Z. Jusys, J. Kaiser, R.J. Behm, Electrooxidation of CO and H2/CO mixtures on a carbon-supported Pt catalyst - a kinetic and mechanistic study by differential electrochemical mass spectrometry, Phys. Chem. Chem. Phys. 3 (2001) 4650–4660, https://doi.org/10.1039/b104617a.
[46] L. Jiang, A. Hsu, D. Chu, R. Chen, Ethanol electro-oxidation on Pt/C and PtSn/C catalysts in alkaline and acid solutions, Int. J. Hydrog. Energy 35 (2010) 365–372, https://doi.org/10.1016/j.ijhydene.2009.10.058.
[47] M. Alsabet, M. Grden, G. Jerkiewicz, Comprehensive study of the growth of thin oxide layers on Pt electrodes under well-defined temperature, potential, and time conditions, J. Electroanal. Chem. 589 (2006) 120–127, https://doi.org/10.1016/j.jelechem.2006.01.022.
[48] H. Kita, S. Ye, A. Aramata, N. Furuya, Adsorption of hydrogen on platinum single crystal electrodes in acid and alkali solutions, J. Electroanal. Chem. 295 (1990) 317–331, https://doi.org/10.1016/0022-0728(90)85025-Z.

[49] N.M. Marković, T.J. Schmidt, B.N. Grgur, H.A. Gasteiger, R.J. Behm, P.N. Ross, Effect of temperature on surface processes at the Pt(111)—liquid Interface: hydrogen adsorption, oxide formation, and CO oxidation, J. Phys. Chem. B 103 (1999) 8568–8577, https://doi.org/10.1021/jp991826u.
[50] E. Morallón, J.L. Vázquez, A. Aldaz, Electrochemical behaviour of Pt(111) in alkaline media. Effect of specific adsorption of anions, J. Electroanal. Chem. 334 (1992) 323–338, https://doi.org/10.1016/0022-0728(92)80581-N.
[51] Y.B. Vassiliev, V.S. Bagotzky, O.A. Khazova, Kinetics and mechanism of formation and reduction of oxide layers on platinum, J. Electroanal. Chem. Interfacial Electrochem. 181 (1984) 219–233, https://doi.org/10.1016/0368-1874(84)83631-x.
[52] A.V. Tripkovi, K.D. Popovi, B.N. Grgur, B. Blizanac, P.N. Ross, N.M. Markovi, Methanol electrooxidation on supported Pt and PtRu catalysts in acid and alkaline solutions, Electrochim. Acta 47 (2002) 3707–3714, https://doi.org/10.1016/S0013-4686(02)00340-7.
[53] D. Abrun, J.L. Cohen, D.J. Volpe, Electrochemical determination of activation energies for methanol oxidation on polycrystalline platinum in acidic and alkaline electrolytes, Phys. Chem. Chem. Phys. 9 (2007) 49–77, https://doi.org/10.1039/b612040g.
[54] B.C. Batista, E. Sitta, M. Eiswirth, H. Varela, Autocatalysis in the open circuit interaction of alcohol molecules with oxidized Pt surfaces, Phys. Chem. Chem. Phys. 10 (2008) 6686–6692, https://doi.org/10.1039/b811787j.
[55] R.J. Behm, Z. Jusys, The potential of model studies for the understanding of catalyst poisoning and temperature effects in polymer electrolyte fuel cell reactions, J. Power Sources 154 (2006) 327–342, https://doi.org/10.1016/j.jpowsour.2005.10.086.
[56] J.V. Perales-Rondón, E. Herrero, J.M. Feliu, On the activation energy of the formic acid oxidation reaction on platinum electrodes, J. Electroanal. Chem. 742 (2015) 90–96, https://doi.org/10.1016/j.jelechem.2015.02.003.
[57] A. Ferre-Vilaplana, C. Buso-Rogero, J.M. Feliu, E. Herrero, Cleavage of the C-C bond in the ethanol oxidation reaction on platinum. Insight from experiments and calculations, J. Phys. Chem. C 120 (2016) 11590–11597, https://doi.org/10.1021/acs.jpcc.6b03117.
[58] J.O. Bockris, A.K.N. Reddy, Modern Electrochemistry 2B: Electrodics in Chemistry, Biology, and Environmental Science, 53, Springer Science & Business Media, 2004 https://doi.org/10.1017/CBO9781107415324.004.
[59] S.Y. Shen, T.S. Zhao, Q.X. Wu, Product analysis of the ethanol oxidation reaction on palladium-based catalysts in an anion-exchange membrane fuel cell environment, Int. J. Hydrog. Energy 37 (2012) 575–582, https://doi.org/10.1016/j.ijhydene.2011.09.077.